Development of an anatomically-based SPH model for cranial ballistic injury

†E.E. Kwon[1], M.R. Singh[1], R.D. Vallabh[1], *R. Das[1], J.W. Fernandez[2,3] and M.C. Taylor[4]

[1]Department of Mechanical Engineering, University of Auckland, New Zealand
[2]Auckland Bioengineering Institute (ABI), University of Auckland, New Zealand
[3]Department of Engineering Science, The University of Auckland, Auckland, New Zealand
[4]The Institute of Environmental Science and Research (ESR), Christchurch Science Centre, New Zealand

*Presenting author: r.das@auckland.ac.nz
†Corresponding author: eryn.kwon@auckland.ac.nz

Abstract

Forensic investigation has the primary challenge of assessing cause from limited evidence. To inform the investigation process, computational modelling can assess: i) the potential ballistic pathways, by analysing entry wound and blood spatter patterns; and ii) the influence of target material effects and cranial geometry. The retrograde ejection of blood and tissue following projectile impact from the entry wound is called 'backspatter' and can aid in informing the investigator about the proximity of the shooter, with the potential to differentiate between suicide and homicide. However, the 'backspatter' phenomenon is not well understood. This study presents (i) the development of an anatomically-based model of cranial ballistic injury using the Smoothed Particle Hydrodynamics (SPH) method; (ii) simulation of the tail splashing and temporary cavitation mechanisms by utilizing a range of scalp and bone simulants and comparison with experiment; (iii) evaluation of cranial stress and strain and energy dissipation; and (iv) evaluation of the effects of bullet characteristics on the creation of the entry wound by parametric analysis.

Keywords: Smooth Particle Hydrodynamics, SPH, Ballistic Simulation, Backspatter

Introduction

Backspatter refers to ejection of biological tissue from ballistic wounds, opposite to the line of fire (Stephens and Allen 1983, Karger 2008). It is widely accepted that backspatter occurs, particularly in close-range contact shots to the head (Stephens and Allen 1983, Yen, Thali et al. 2003). The stain patterns resulting from backspatter are of critical importance in a crime scene because of the direction against the line of fire (Grosse Perdekamp, Vennemann et al. 2005), providing a potential connection between the victim and the shooter. However, the literature on backspatter is limited compared to other areas of blood spatter research, providing a less solid foundation and a less thorough understanding of the mechanisms (Radford 2009).

The three main mechanisms contributing to backspatter reported in the literature are (i) subcutaneous gas pockets; (ii) temporary cavities; and (iii) tail splashing (Karger 2008). Subcutaneous gas pockets are temporary spaces between skin and bone created due to muzzle gas from contact or near-contact shots (Karger and Brinkmann 1997). Temporary cavities form when the passage of a projectile through near-water density organs, such as the musculature or the brain, creates pressure waves to radially expend the bullet trail temporarily (Karger 2008). In the case of distant shots, the temporary cavity in brain is believed to be a major contributor(Foote 2012). Tail splashing results from a backward streaming of fluid and fragments along the sides of the bullet in the retrograde direction upon projectile impact (Amato, Billy et al. 1974).

Due to the extreme speed of a projectile, the ballistic event happens very quickly, making study of the backspatter event difficult, with little prior work collecting detailed physical evidences to allow thorough validation. Additionally, the backspatter event is the result of various combinations of mechanisms and variables, making it difficult to isolate each mechanism to gauge their contribution. To reduce the complexity issues, this study focuses only on distant shots, so the subcutaneous gas pocket mechanism can be eliminated from consideration. The focus of this research is solely on the tail splash and temporary cavitation.

In order to collect the necessary detailed physical evidences, it is essential to form proper models, as human samples are not viable due to ethical issues. Previous literature has shown that the problem of finding a target for experimentation that best simulates the properties of the human cranium has been a significant constraint with much controversy. The use of animal models, involving calves or swine has been established well in the literature (Karger, Nusse et al. 1996, Karger, Nusse et al. 1997, Karger, Nusse et al. 2002, Radford 2009). The animal models used commonly have ethical issues, different geometry to that of a human cranium, and individual biodiversity which makes them unreliable as an experimental model (Yen, Thali et al. 2003). To provide an alternative to the animal models, physical models using synthetic materials have been developing, with increased geometric details and complexity in their construction (Stephens and Allen 1983, Thali, Kneubuehl et al. 2002, Radford 2009, Foote 2012, Carr, Lindstrom et al. 2014, Kwon 2014). Physical models have no ethical issues and the experimental results agree well with the reported human case studies (Thali, Kneubuehl et al. 2002, Carr, Lindstrom et al. 2014). However, the high cost of each sample and the manufacturing difficulties are major hurdles to using physical models to study backspatter.

Computational models are increasingly being used as an alternative to complicated, costly, and potentially ethically challenging experiments. In ballistic experiments, the experimental parameters, such as speed of the bullet or the sample material properties, are not easily controlled. However, the computational model allows fast and easy customisation of the experimental parameters. This gives the computational model a clear advantage for forensic crime scene reconstructions, where the bullet calibre or the impact speed is not known, or the victim had significantly different biological material properties due to aging or disease. For example, if the victim was suffering from osteoporosis (a disease effecting bone density, causing weak and brittle bones), the current studies in animal or physical models would have to be re-done to compensate for this factor. The computational model has unmatched analytic advantage as the each layer of the model can be visualised separately without damaging the other layers. For animal or physical models, the skin layer must be damaged in order to analyse the bone layer defect size and crack propagation.

There are two computational methods through which study of backspatter could be made possible: finite element method (FEM) and Smoothed Particle Hydrodynamics (SPH). FEM offers the advantage of being able to model structures with intricate shapes and indirectly quantify their complex behaviour at a point (Raul, Deck et al. 2007). However, this method has a significant limitation in that at high speeds and deformations, mesh integrity is lost. In contrast, SPH, originally developed for astrophysics (Gingold and Monaghan 1977), is a conservative, mesh-less method that can handle complicated, highly-deformable geometry, large void areas, and dynamic ballistic behaviour (Stellingwerf and Wingate 1993). The SPH method has been utilized in several applications, including explosive fragmentation of metal casings involving intense shock and high rate plastic deformation (Kong, Wu et al. 2013) and the high speed impact of a metal sphere on a thin metallic plate with a range of materials and velocities (Kalameh, Karamali et al. 2012).

In this study we present both a simple flat plate SPH model as well as an anatomically accurate SPH model of the male human head. The less-computationally-expensive simple geometry is used to test various material constitutive models and different simulants, as well as ballistic characteristics. The anatomical geometry was used for the final models, which represent a more detailed and realistic ballistic simulation. Both geometries consist of two layers: the scalp and the skull. The scalp comprises of the skin and the connective tissues overlying the top of the head (Harris, Yoganandan et al. 1993). The skin is a highly non-linear, anisotropic, viscoelastic and nearly incompressible material (Crichton, Donose et al. 2011, Crichton, Chen et al. 2012). The skull is the firm bone that encases the brain. On projectile impact, the skull is expected to show radial fractures originating from the point of impact and concentric fractures around the bullet entry and exit sites (Viel, Gehl et al. 2009). Common characteristics often observed but not always present, include bevelling and keyhole defects (Quatrehomme and Iscan 1997). Another major layer of the human cranium, the brain, has been omitted in this research to concentrate the investigation on the contribution of scalp and skull to backspatter generation.

In this paper, we present findings of the SPH-based simple and anatomically-accurate model of cranial ballistic injury, including: (i) simulation of the tail splashing and temporary cavitation mechanisms, utilizing a range of scalp and bone simulants and comparison with experiment; (ii) evaluation of cranial stress and strain and energy dissipation; and (iii) evaluation of the effects of bullet calibre and speed on the creation of the entry wound by parametric analysis.

Methods

The simple plate geometry (Figure 1) is composed of two flat plates of 100 x 100 x 5 mm, each representing the scalp layer and the skull layer of a human cranium. The minimum SPH particle size for this geometry was 0.7 mm, which contained ~ 580,000 SPH particles.

A representative scalp and cranium geometry was adapted from the Physiome Project repository of a 38 year old male from the Visible Human male data set (Spitzer, Ackerman et al. 1996) and developed at the Auckland Bioengineering Institute. The dimensions of the scalp layer were acquired from MRI scan results taken from images from the Centre from Advanced MRI (Auckland University). The SPH particle size was set to 2.5 mm, which contained ~141,000 SPH particles.

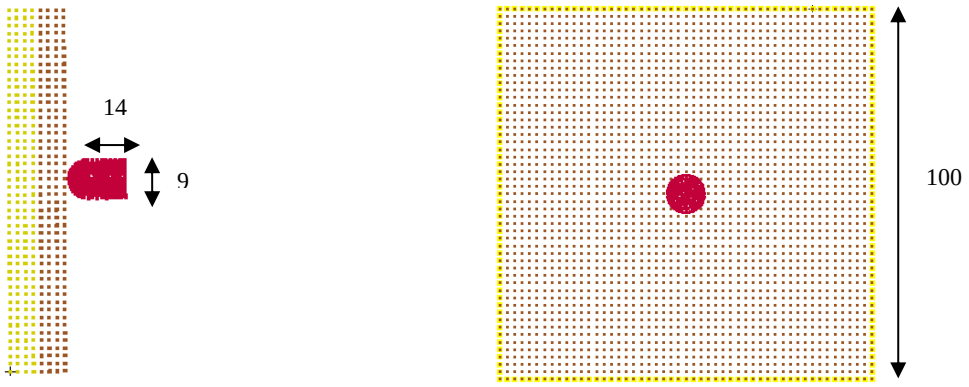

Figure 1. Simple geometry with a 9 mm bullet, Scalp layer is shown as red, Skull layer is shown as yellow, the pinned boundary is shown as yellow edge on the right

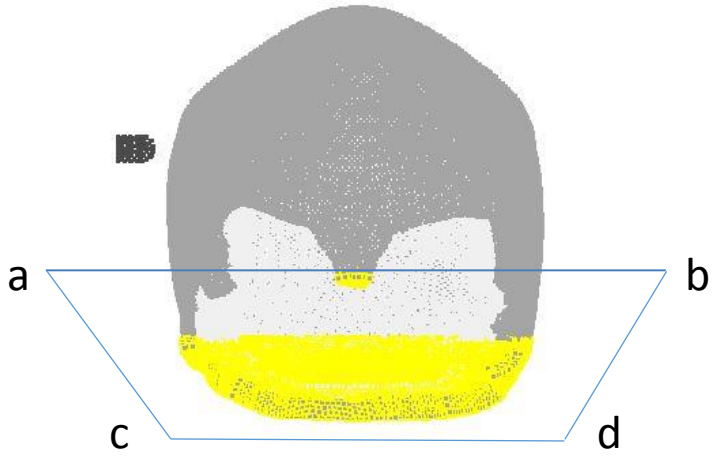

Figure 2. Anatomical geometry with a 9 mm bullet, scalp is shown in grey, skull is shown in white, the pinned boundary below the plane abcd is highlighted with yellow

Both geometries had equivalent physical models, with matching geometry and simulant materials. The experimental result was recorded using high speed photography, at a frame rate of 30,000 frames per second. The purpose of the physical models was to be the validation tool for the computational models.

A total of 16 scalp-skull simulant combinations, consisting of four scalp simulant and four skull simulant materials, were simulated using the simple geometry model. For the scalp simulants, the material properties of the ballistic gelatine, Room Temperature Vulcanizing (RTV) silicone_1, RTV silicone_2 and natural rubber were modelled using either viscoelastic or hyperelastic failure. The material constants were obtained from either the Mooney-Rivlin or the Yeoh models (Wang, Deng et al. 2004, Korochkina, Jewell et al. 2008). Both models use strain energy potential to characterise rubber. For the skull simulants, the material properties of the Medium-Density Fiberboard (MDF), Particle board, Polyurethane_1 and Polyurethane_2 were modelled using isotropic-elastic failure. No material constants were required for the elastic failure.

The anatomical geometry model was simulated using the best performing simulants selected based on the simple geometry model simulation results. The scalp layer was modelled using RTV silicone_2 and the skull layer was modelled using Polyurethane_2.

The simple geometry model was also used for the parametric studies of the effect of bullet calibre and the velocity on ballistic response of the target. 2 different types of bullets were used, a 9 mm Luger and a .22 Long Rifle (LR). The 9 mm is a 115grain, Full Metal Jacket, and has solid lead core with a copper gilding material coating. The .22 LR had less wounding potential and penetrating potential compared to the 9 mm Luger. Both the 9 mm and .22 bullets were modelled as a cylinder with hemisphere tip, with material properties of copper and density of lead to represent the solid lead core. The bullet was modelled using Johnson and Cook high velocity impact copper model from ANSYS material library (Johnson and Cook 1985).

The 9 mm was simulated with 300 m/s and 370 m/s impact velocity, each representing the lower limit and the upper limit of the projectile speed respectively. In ballistic experimentation, the physical models were shot from a distance over 1 m. This isolated the tail splashing and temporary cavitation as backspatter generation mechanisms by eliminating the subcutaneous gas pockets that would have formed if the shot distance were to be closer. As seen in Figures 1 and 2, the bullet has been positioned at the centre of the simple geometry model and on the right temple of the

anatomical geometry model. The anatomical position was chosen based on the frequency of the cranial ballistic wounding site.

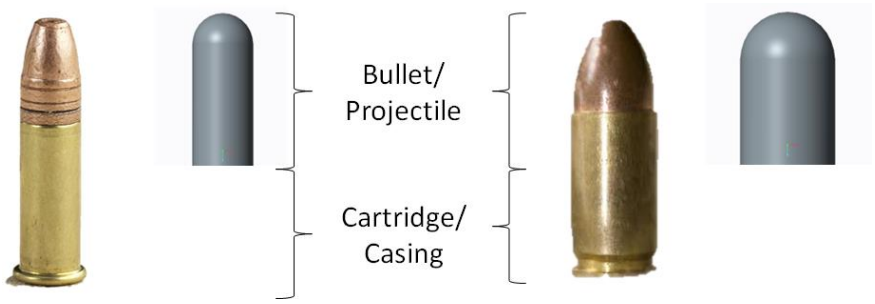

Figure 3. Physical and computational bullet geometry comparison between 0.22 (left) and 9 mm (right) – only the projectile part is modelled in computational models

Results and Discussion

Simple geometry

The experimental and simulation results were analysed to determine the most suitable scalp and skull simulant combination to represent human cranial ballistic wounding. The simulation results were validated by comparison to the experimental results. The comparison was based on both qualitative and quantitative observations made over dynamic deformation behaviour and static defect dimensions and characteristics. Two of the most typical dynamic ballistic deformation results from the testing and simulation of the physical and computational models are compared chronologically in Figures 4 and 5.

The first main point of analysis was the ability to replicate the tail splash and temporary cavitation backspatter generation mechanisms. The gelatine skin simulant was better at demonstrating the tail splashing mechanism than any other scalp simulants used. The tail splash from the Gelatin-Polyurethane_1 model is illustrated, at 0.1 ms post-impact, in Figure 4 (a) and (e). On the other hand, the Silicone_1-Polyurethane_2 model illustrates the subcutaneous temporary cavity mechanism very well. The computational model successfully simulated the retrograde elastic bulging of the scalp simulant as well as the reduction of the bullet entry hole size. The choice of skull simulants affected the magnitude of the ballistic response, producing more backspatter for the Polyurethane simulants compared to the MDF or Particle Board. Also, there was minimal skull simulant backspatter observed, which concurs with the literature findings (Burnett 1991, Coupland, Rothschild et al. 2011).

It is expected that the tough integument of the human scalp will prevent the crushed tissues to backspatter as freely as the gelatine simulant. Therefore, the Silicone_2 was accepted as the best scalp simulant. The human skulls also show bevelling and minor crack formation at the bullet entrance, and the lack of ability to produce such characteristics eliminated both the MDF and Particle Board as a viable skull simulant. The Polyurethane_2 was chosen as the best skull simulant based on the bone defect diameter and morphology.

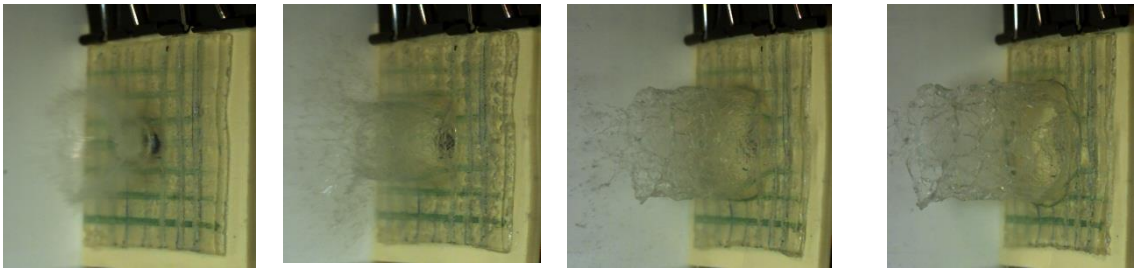

(a) 0.1 ms (b) 0.3 ms (c) 0.7 ms (d) 1 ms

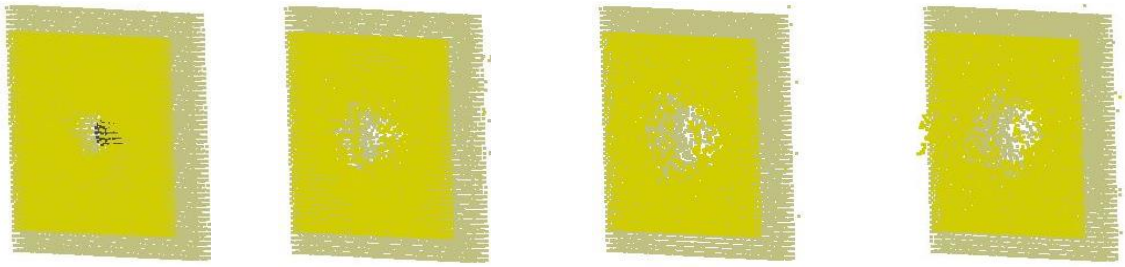

(e) 0.1 ms (f) 0.3 ms (g) 0.7 ms (h) 1 ms

Figure 4. Comparison of experimental (a-d) and simulation (e-h) results of a 9 mm projectile impact on Gelatin-Polyurethane_1 model

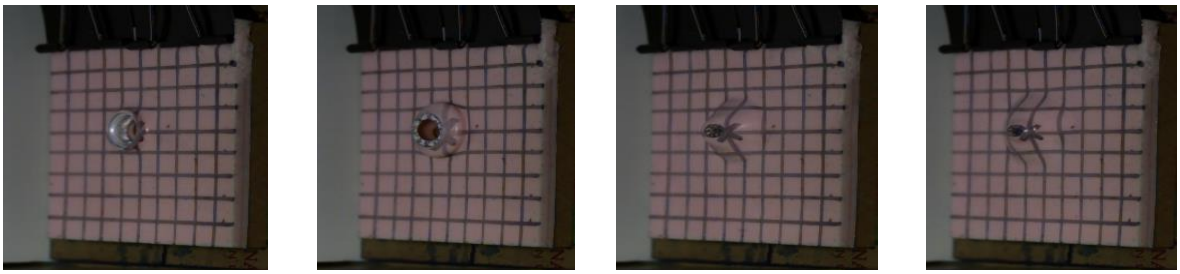

(a) 0.1 ms (b) 0.3 ms (c) 0.7 ms (d) 1 ms

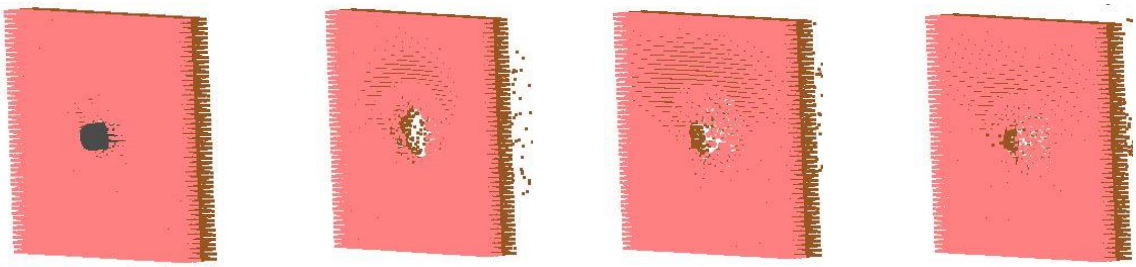

(e) 0.1 ms (f) 0.3 ms (g) 0.7 ms (h) 1 ms

Figure 5. Comparison of experimental (a-d) and simulation (e-h) results of a 9 mm projectile impact on Silicone_1-Polyurethane_2 model

Anatomical geometry
The anatomical geometry model simulated using the Silicone_2-Polyurethane_2 simulant combination produced an extended subcutaneous temporary cavity, due to surface curvature and increased kinetic energy absorption. This increased magnitude of temporary cavity dynamics illustrated the existence of a delayed backspatter due to the temporary cavity mechanism. Crucially, the tail splash mechanism produced backspatter at the early impact stage, and the anatomical geometry model produced a chronologically separated second ejection of the backspatter. This delayed backspatter was observed around 2.6 ms and coincided with the collapse of the temporary cavity. Therefore, the pressure created by the collapse of the temporary cavity mechanism is responsible for the retrograde ejection of the fragments inside the cavity of this backspatter via path of least resistance (Figure 6).

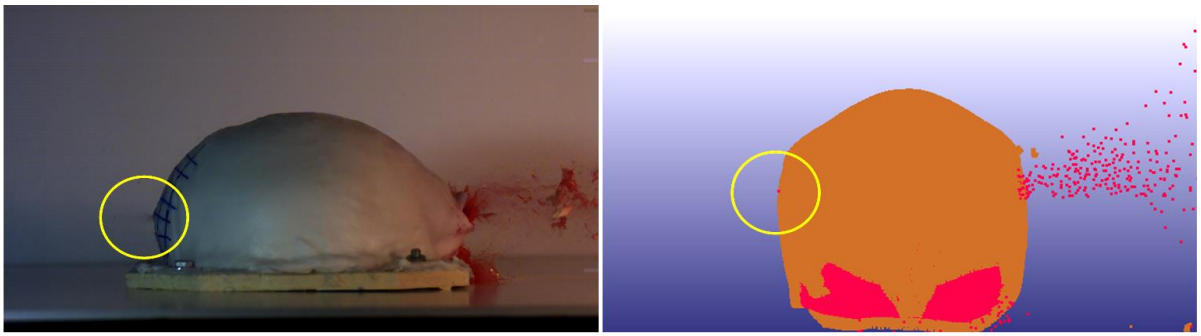

Figure 6. Comparison of experimental (left) and simulation (right) results of a 9 mm projectile impact on Silicone_2-Polyurethane_2 anatomical geometry model, at 2.6 ms post-impact. The delayed backspatter is highlighted with yellow circles.

Computational model unique analysis
One of the main advantages of the simulation is that it allows detailed analysis of the impact event without the use of complicated actuators and associated error. In experimentation, it is almost impossible to isolate the stress and strain developed in each layer of the cranial model. For the aforementioned practical reasons, there has been no analysis on the stress patterns developed in an animal model nor a physical model reported in a literature previously.

However, the computational modelling has ability to calculate the stress and strain of the target without additional processing. The anatomical geometry model simulation result was analysed for the Von Mises Stress (Figure 7) and Plastic strain (Figure 8). These are typical engineering measurements used to analyse stressed and deformation developed in a structure. The plastic strain was useful to monitor the area of the deformation while the Von Mises stress was used to visualise stress distribution in the bone layer.

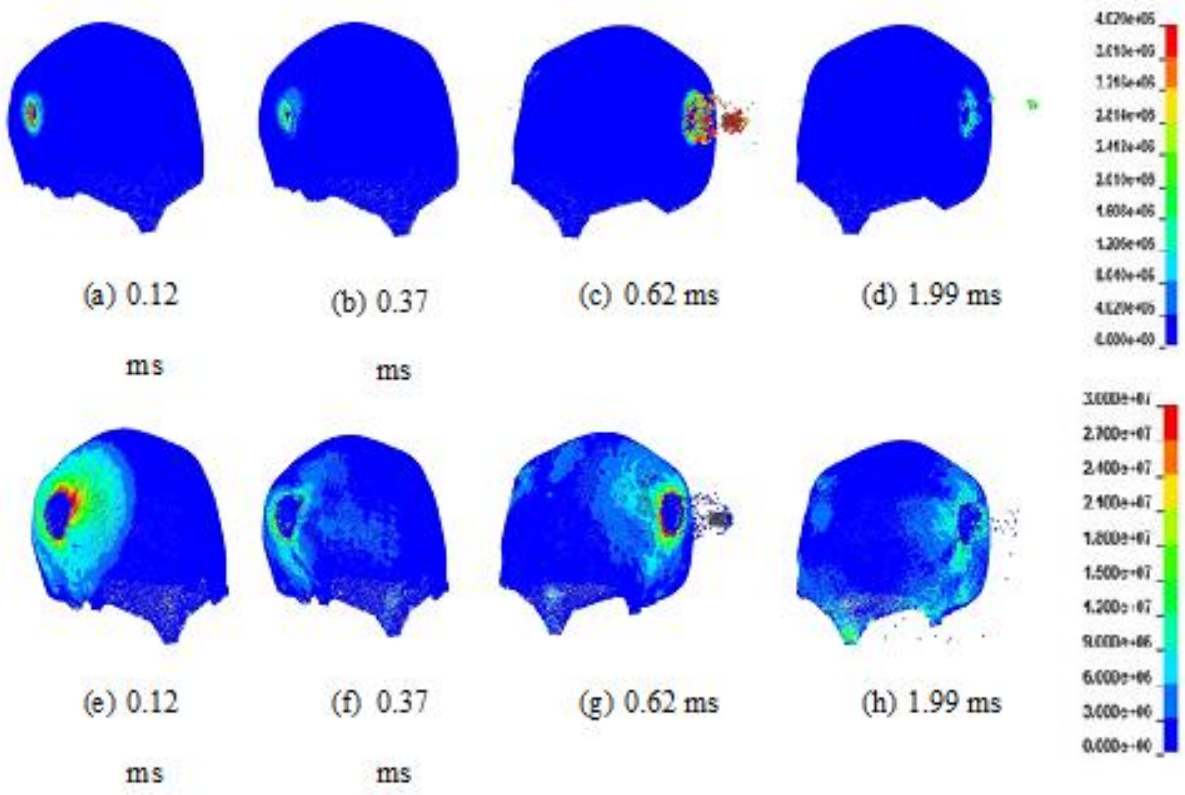

Figure 7. Evolution of Von Mises stresses on the scalp (a-d) and the skull (e-h) of the anatomical geometry model

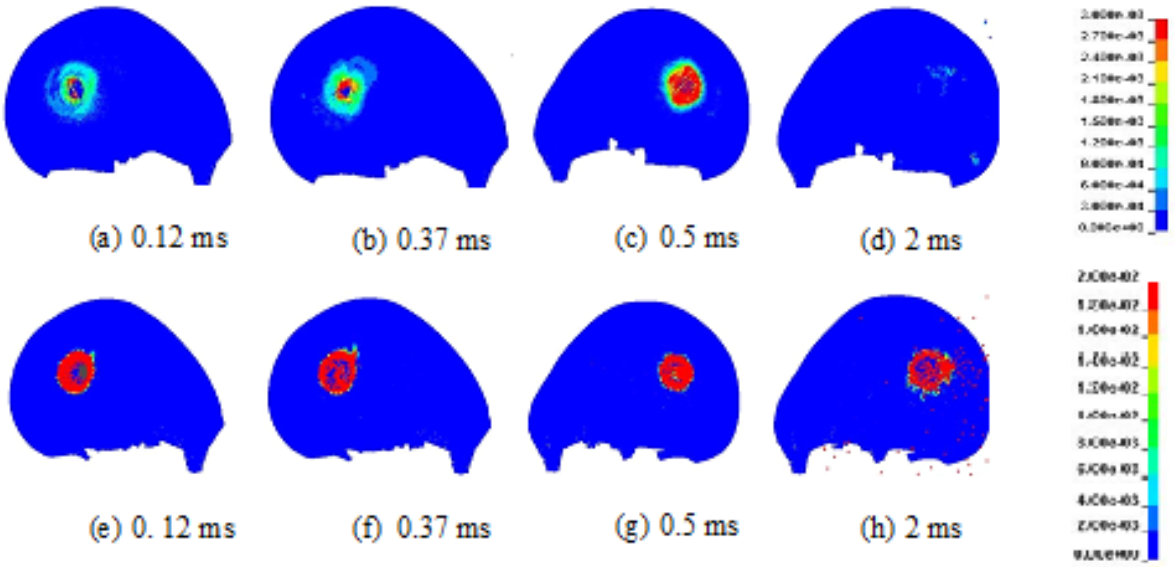

Figure 8. Evolution of mean effective strain on the scalp (a-d) and the skull (e-h) of the anatomical geometry model

For the stress analysis, the Silicone_2 scalp simulant stretches and fails at the impact point immediately upon the projectile impact. This is due to the high stresses generated around the entry site as shown in Figure 7 (a). A maximum stress of 4.02 MPa is generated at the bullet entry site, which is greater than the tensile strength of the material, leading to extension and failure. This is in accordance with the observations made by Jussila et al (Jussila, Leppaniemi et al. 2005), who assert that 'an impacting bullet makes the skin to stretch, partially crush and finally rupture, allowing the bullet to enter underlying tissue'. The impact stresses are localized and most of the surrounding areas of the head are not affected, as indicated by the blue regions. At a time of 0.3 ms, Figure 7 (b), the entrance cavity oscillates and closes up, causing build-up of high pressures. Following the exit of the bullet shown in Figures 7 (c) and 7 (d), the hyperelastic nature of the material leads to minor oscillations as it tries to recover to its original state and close up the cavity.

On bullet impact, high stresses in the order of 30 MPa are produced in the Polyurethane_2 skull simulant. Since the stresses are greater than the ultimate tensile strength of the resin it fails at the impact point in a brittle manner. The stresses then radiate outwards as shown in Figure 7 (e) and 7 (f). The magnitude of the radiating stresses (4-10 MPa) is well below the failure stress of the material. High stresses produced at the exit site initiate crack propagation along the cranium as indicated by the faint red lines in Figures 7 (g) and 7 (h). The entry site presents a clean 'punched out' external appearance while the exit wound is much larger and irregular in shape. This is the desired result supported by other sources in literatures (Quatrehomme and Iscan 1998, Quatrehomme and Iscan 1999).

For the strain analysis, the Silicone_2 scalp simulant strains and starts tearing as shown in Figure 8 (a). A similar tearing of the skin from a contact shot has been recorded in literature (Faller-Marquardt, Bohnert et al. 2004). Even after failure, the Silicone_2 tries to close up the entrance wound causing the surrounding material to strain as indicated by the light blue particles in Figure 8 (b). The elastic deformation of the silicone rubber on bullet exit can be clearly perceived by the red regions in Figure 8 (c). Over time, the oscillations die away and the strain diminishes as shown in Figure 8 (d).

When the bullet enters the Polyurethane_2 skull layer of the model, strains up to 2% are observed at the impact point leading to fracture. In addition, the high strains caused around bullet entry and exit sites in Figures 8 (f) and 8 (h) are much larger than the bullet diameter. An implication of this observation is that the polyurethane resin demonstrates some amount of plastic deformation and is therefore not perfectly brittle.

The energy graph of each part and layers involved (Figure 9) provides a very valuable insight into the ballistic impact event. It shows how the original kinetic energy of the bullet is converted to various other forms of energy to result in the ballistic response of the target as a whole. Initially, the particles that shape the scalp and cranium layers are at rest (Point A and Origin). On impact (energy change to point B and E), it is assumed that the bullet's kinetic energy changes into: bullet deformation energy, damage energy, heat generation, and impact energy (Komuński, Kubiak et al. 2009). Since the bullet used in experimentation has a full metal jacket it is assumed not to lose energy due to bullet deformation. Energy lost in the form of heat is thought to be minimal in our analysis.

The scalp and cranium layers each absorb 50-60J of energy as the bullet passes through (Point E). The rest of the energy (117J, point A to point B in Figure 9) is used to fracture and damage the material. Between points E and F, the total energy of the cranial layer remains fairly constant, but

the scalp loses a fraction of its energy. A similar effect is observed between points F and G as the scalp layer gains 50J of energy and then loses a small percentage of it.

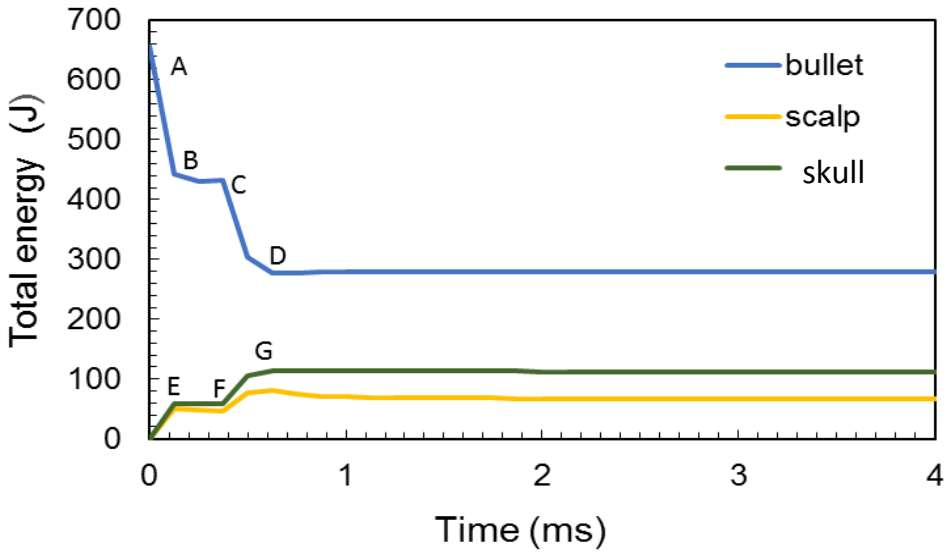

Figure 9. The total energy of the bullet, scalp and skull over time

This behaviour can be best explained by considering the total energy absorbed by the hyperelastic scalp over time in relation to its internal energy, as shown in Figure 10. Due to its elastic nature, a fraction (5J) of the total internal energy (25J) at 0.12ms is utilized in deforming the material as it tries to recover to its original state (Point E and F). Thus, the scalp loses 20% (5J/25J) of its internal energy in the form of strain energy. Once the scalp layer partially recovers to a position of equilibrium, it stops oscillating and the total energy of the system remains constant over time. The cranium is represented by a hard, brittle material so it sustains its internal energy after bullet exit (Point G and beyond) without further deformation. In summary, a total of 380J of energy is lost by the projectile, while the scalp and cranium layers gain 66J (17.4% of projectile energy) and 112J (29.5%) respectively. The scalp layer loses 20% of its internal energy due to straining of the material.

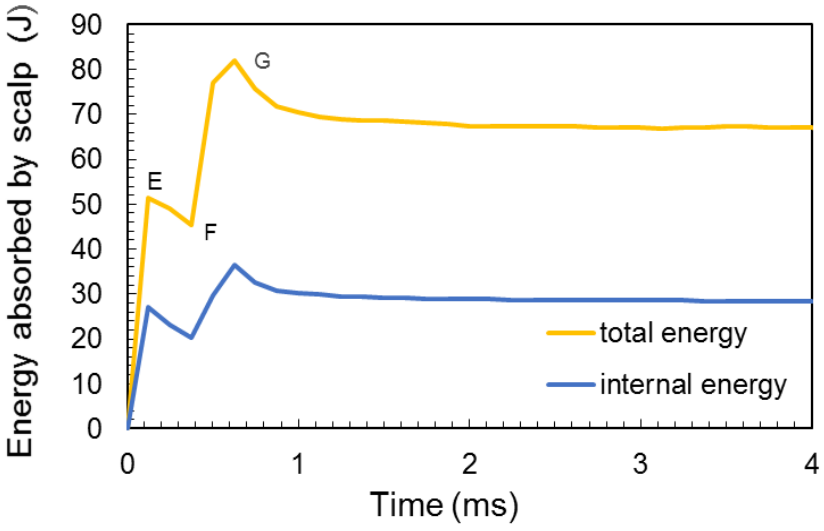

Figure 10. Comparison of the scalp layer internal energy to its total energy

The ballistic parametric study showed that the larger calibre bullet produces the larger defect size, which concurs with the experimental observations. The simulation produced similar defect characteristics for the bone layer, producing bevelling and keyhole defect of similar dimensions (Figure 11).

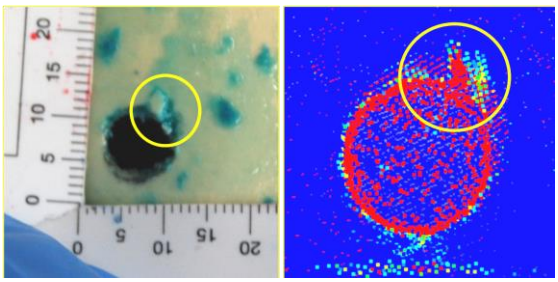

(a) Physical model (a) Computational model

Figure 11. Comparison between the bone layer keyhole defect of (a) physical and (b) computational (anatomical geometry) model

Bullet characteristic parametric study

The calibre and speed of the projectile used was varied in the anatomical geometry model to investigate the dependence of bullet characteristics on the backspatter generation and the stress/strain developed in the model.

The .22 LR produced entrance defect smaller than the 9 mm. Also the stress generated by the .22 LR was more localized on the impact site. More significantly, the .22 LR impact did not produce any backspatter from both the physical and computational models.

The bullet speed change does not have a physical experimental result to compare to. The simulational observation was: i) higher impact speed of 370 m/s resulted in larger area of stress development with greater impact stresses for both the .22 LR and the 9 mm; ii) The percentage energy absorbed from the projectile was almost independent of the impact velocity. This signifies more energy is absorbed into the target as the projectile speed increases. In an experimental study by Clemedson et al. (Clemedson, Falconer et al. 1973), the maximum pressure created in the head varied by approximately the square of the projectile velocity.

Conclusions

This study presents both a simplified and anatomically-accurate computational models of human cranium for ballistic backspatter research. The computational model successfully incorporated human anatomical geometry into the scalp and the skull layers. The simple geometry was used to increase simulational efficiency in simulant evaluation.

The tail splash and temporary cavitation mechanism has been witnessed and confirmed as a major backspatter cause/mechanism when the subcutaneous gas pocket mechanism was eliminated. When combined with the unique ability of the computational models to provide the stress, strain and energy graphs, a detailed chronological description of the temporary cavitation mechanism was made, which was not reported in literatures before.

The effect of the bullet calibre or speed change resulted in desired variation in the simulational results.

Overall, the computational model has these benefits

- No ethical issue
- Cost-effective
- Ease of experimentation
- Higher control of experimental variables
- Ease of customisation for the use of forensic case studies and crime reconstructions
- Unmatched analytical advantage, providing otherwise unattainable values such as stress, strain and energy of individual parts.
- Non-invasive analysis

References

Amato, J. J., L. J. Billy, N. S. Lawson and N. M. Rich (1974). "High Velocity Missile Injury: An Experimental Study of the Retentive Forces of Tissue." The American Journal of Surgery **127**: 454-459.

Burnett, B. R. (1991). "Detection of Bone and Bone-Plus-Bullet Particles in Backspatter from Close-Range Shots to Heads." Journal of Forensic Science **36**(6): 1745-1752.

Carr, D., A.-C. Lindstrom, A. Jareborg, S. Champion, N. Waddell, D. Miller, M. Teagle, I. Horsfall and J. Kieser (2014). "Development of a skull/brain model for military wound ballistics studies." International Journal of Legal Medicine: 1-6.

Clemedson, C.-J., B. Falconer, L. Frankenberg, A. Jönsson and M. D. J. Wennerstrand (1973). "Head injuries caused by small-calibre, high velocity bullets." Zeitschrift für Rechtsmedizin **73**(2): 103-114.

Coupland, R. M., M. A. Rothschild, M. J. Thali, B. P. Kneubuehl, R. M. Coupland, M. A. Rothschild and M. J. Thali (2011). Introduction to Wound Ballistics. B. P. Kneubuehl, Springer Berlin Heidelberg**:** 1-2.

Crichton, M. L., X. Chen, H. Huang and M. A. F. Kendall (2012). "Elastic modulus and viscoelastic properties of full thickness skin characterised at micro scales." Biomaterials.

Crichton, M. L., B. C. Donose, X. Chen, A. P. Raphael, H. Huang and M. A. F. Kendall (2011). "The viscoelastic, hyperelastic and scale dependent behaviour of freshly excised individual skin layers." Biomaterials **32**(20): 4670-4681.

Faller-Marquardt, M., M. Bohnert and S. Pollak (2004). "Detachment of the periosteum and soot staining of its underside in contact shots to the cerebral cranium." Int J Legal Med **118**(6): 343-347.

Foote, N. R. (2012). The Role of the Temporary Cavity in Cranial Backspatter. Master of Science in Forensic Science, The University of Auckland.

Gingold, R. A. and J. J. Monaghan (1977). "Smoothed particle hydrodynamics-theory and application to non-spherical stars." Monthly notices of the royal astronomical society **181**: 375-389.

Grosse Perdekamp, M., B. Vennemann, D. Mattern, A. Serr and S. Pollak (2005). "Tissue defect at the gunshot entrance wound: what happens to the skin?" Int J Legal Med **119**(4): 217-222.

Harris, G. F., N. Yoganandan, D. Schmaltz, J. Reinartz, F. Pintar and A. Sances Jr (1993). "A biomechanical impact test system for head and facial injury assessment and model development." Journal of Biomedical Engineering **15**(1): 67-73.

Johnson, G. R. and W. H. Cook (1985). "Fracture characteristics of three metals subjected to various strains, strain rates, temperatures and pressures." Engineering Fracture Mechanics **21**(1): 31-48.

Jussila, J., A. Leppaniemi, M. Paronen and E. Kulomaki (2005). "Ballistic skin simulant." Forensic Sci Int **150**(1): 63-71.

Kalameh, H. A., A. Karamali, C. Anitescu and T. Rabczuk (2012). "High velocity impact of metal sphere on thin metallic plate using smooth particle hydrodynamics (SPH) method." Frontiers of Structural and Civil Engineering **6**(2): 101-110.

Karger, B. (2008). Forensic Ballistics. Forensic Pathology Reviews. M. Tsokos. Totowa, NJ, Humana Press. **5:** 139-172.

Karger, B. and B. Brinkmann (1997). "Multiple gunshot suicides: potential for physical activity and medico-legal aspects." Int J. Legal Med. **10**: 188-192.

Karger, B., R. Nusse and T. Bajanowski (2002). "Backspatter on the Firearm and Hand in Experimental Close-Range Gunshots to the Head." The American Journal of Forensic Medicine and Pathology **23**(3): 211-213.

Karger, B., R. Nusse, G. Schroeder, S. Wustenbecker and B. Brinkmann (1996). "Backspatter from Experimental Close-Range Shots to the Head I-Macrobackspatter." International Journal of Legal Medicine **109**: 66-74.

Karger, B., R. Nusse, H. D. Troger and B. Brinkmann (1997). "Backspatter from Experimental Close-Range Shots to the Head II-Microbackspatter and the Morphology of Bloodstains." International Journal of Legal Medicine **110**: 27-30.

Komuński, P., T. Kubiak, M. Ładwijt and R. Romek (2009). "Energy transmission from bullet impact onto head or neck through structures of the protective ballistic helmet-tests and evaluation." Techniczne Wyroby Włókiennicze **17**: 18-23.

Kong, X., W. Wu, J. Li, F. Liu, P. Chen and Y. Li (2013). "A numerical investigation on explosive fragmentation of metal casing using Smoothed Particle Hydrodynamic method." Materials & Design **51**: 729-741.

Korochkina, T. V., E. H. Jewell, T. C. Claypole and D. T. Gethin (2008). "Experimental and numerical investigation into nonlinear deformation of silicone rubber pads during ink transfer process." Polymer Testing **27**(6): 778-791.

Kwon, E. E. (2014). Development of Physical and Numerical Models to Study Cranial Backspatter. Master of Engineering, University of Auckland.
Quatrehomme, G. and M. Y. Iscan (1997). "Bevelling in exit gunshot wounds in bones." Forensic Sci Int **89**(1-2): 93-101.
Quatrehomme, G. and M. Y. Iscan (1998). "Gunshot wounds to the skull: comparison of entries and exits." Forensic Sci Int **94**(1-2): 141-146.
Quatrehomme, G. and M. Y. Iscan (1999). "Characteristics of gunshot wounds in the skull." J Forensic Sci **44**(3): 568-576.
Radford, G. E. (2009). Modelling Cranial Gunshot Wounds and Backspatter. Master of Science, University of Otago.
Raul, J., C. Deck, F. Meyer, A. Geraut, R. Willinger and B. Ludes (2007). "A finite element model investigation of gunshot injury." International Journal of Legal Medicine **121**: 143-146.
Spitzer, V., M. J. Ackerman, A. L. Scherzinger and D. Whitlock (1996). "The visible human male: a technical report." Journal of the American Medical Informatics Association **3**(2): 118-130.
Stellingwerf, R. and C. Wingate (1993). "Impact modeling with smooth particle hydrodynamics." International Journal of Impact Engineering **14**(1): 707-718.
Stephens, B. G. and T. B. Allen (1983). "Back Spatter of Blood from Gunshot Wounds - Observations and Experimental Simulation." Journal of Forensic Sciences **28**(2): 437-439.
Thali, M. J., B. P. Kneubuehl and R. Dirnhofer (2002). "A "Skin-skull-brain" Model for the Biomechanical Reconstruction of Blunt Forces to the Human Head." Forensic Science International **125**: 195-200.
Viel, G., A. Gehl and J. P. Sperhake (2009). "Intersecting fractures of the skull and gunshot wounds. Case report and literature review." Forensic science, medicine, and pathology **5**(1): 22-27.
Wang, W., T. Deng and S.-g. ZHAO (2004). "Determination for Material Constants of Rubber Mooney-Rivlin Model [J]." Special Purpose Rubber Products **4**: 003.
Yen, K., M. J. Thali, B. P. Kneubuehl, O. Peschel, U. Zollinger and R. Dirnhofer (2003). "Blood-Spatter Patterns: Hands Hold Clues for the Forensic Reconstruction of the Sequence of Events." American Journal of Forensic Medicine and Pathology **24**(2): 132-140.